Mean-Square Radius of Gyration of Oligo- and Polystyrenes in Dilute Solutions

Toshiki Konishi, Takenao Yoshizaki, Toshiya Saito, Yoshiyuki Einaga, and Hiromi Yamakawa*

Department of Polymer Chemistry, Kyoto University, Kyoto 606, Japan.
Received May 30, 1989; Revised Manuscript Received July 8, 1989

ABSTRACT: The apparent mean-square radius of gyration, $\langle S^2 \rangle_s$, was measured by small-angle X-ray scattering for 12 samples of atactic oligo- and polystyrenes (a-PS) in the range of weight-average molecular weight M_w from 578 (pentamer) to 97 300 in cyclohexane at 34.5 °C (Θ temperature). The mean-square radius of gyration $\langle S^2 \rangle$ for the chain contour was calculated from the values of $\langle S^2 \rangle_s$ thus obtained by making correction for the finite thickness of the polymer chain. The ratio of $\langle S^2 \rangle$ to the weight-average degree of polymerization rather steeply increased with increasing M_w and leveled off at M_w higher than 10^5. The theory based on the helical wormlike (HW) chain model described quantitatively the observed results, yielding the values of the model parameters which are in good agreement with those determined from the molecular weight dependence of the mean-square optical anisotropy, $\langle \Gamma^2 \rangle$, and also of the intrinsic viscosity, $[\eta]$. It was found that the Flory–Fox factor, Φ, increased steeply as M_w was decreased from 10^5. This behavior was also in quantitative agreement with the HW theory prediction, while the theory for the Gaussian chain failed to explain it, reflecting the non-Gaussian character of the short a-PS chain in solution.

Introduction

In our previous papers,[1,2] we have studied the mean-square optical anisotropy, $\langle \Gamma^2 \rangle$, and intrinsic viscosity, $[\eta]$, of atactic polystyrene (a-PS) over a wide range of molecular weight including the oligomer region. Applying the corresponding theories[3-6] on the basis of the helical wormlike (HW) chain model to the observed results, we have determined the model parameters for a-PS as the HW chain. These are the differential-geometrical curvature, κ_0, and torsion, τ_0, of the regular helix, namely the characteristic helix, that the HW chain contour becomes at the minimum zero of its elastic energy, the static stiffness parameter, λ^{-1}, and the shift factor M_L defined as the molecular weight per unit contour length. The values obtained for the model parameters have made it possible to picture the characteristic helix of the a-PS chain and its average conformation in dilute solutions. The global properties $\langle \Gamma^2 \rangle$ and $[\eta]$ have also been successfully correlated to the local structure of a-PS in solution on the length scales of the monomer unit for the former and of the four monomer units for the latter.

The present paper extends the study to the (unperturbed) mean-square radius of gyration, $\langle S^2 \rangle$, of a-PS at infinite dilution. In so doing, the small-angle X-ray scattering (SAXS) method was applied to cyclohexane solutions of the same a-PS samples of narrow molecular weight distribution and fixed stereochemical composition (the fraction of racemic diads, $f_r = 0.59 \pm 0.01$). (Note that each sample is a mixture of stereoisomers, so that the fluctuation in f_r is dependent on molecular weight even if f_r itself is not.) Thus the main purpose is to confirm that the HW model theory may explain consistently the behavior of $\langle S^2 \rangle$, $\langle \Gamma^2 \rangle$, and $[\eta]$ of a-PS over a wide range of molecular weight in terms of its local chain conformation.

When we look over the existing literature, we notice that the procedure of determining $\langle S^2 \rangle$ by the SAXS method has not fully been established as yet and still is developing.[7] Thus, in the next two sections, we describe rather in detail our procedure of the SAXS measurement and data processing used in this work. An apparent mean-square radius of gyration determined directly by the scattering methods such as SAXS, small-angle neutron scattering (SANS), and light scattering (LS), which we designate by $\langle S^2 \rangle_s$, includes in principle the contribution of the squared radius of gyration S_c^2 of the cross section of the real polymer chain with finite volume. This effect of the chain thickness becomes progressively large as the molecular weight of the polymer sample goes down to the oligomer region. We must therefore extract $\langle S^2 \rangle$ for the chain contour from $\langle S^2 \rangle_s$ in order to compare the former with its theoretical values. The method for the evaluation of $\langle S^2 \rangle$ is given in the Discussion. Then, the ratios of $\langle S^2 \rangle$ to the weight-average degree of polymerization, x_w, are analyzed by the use of the HW model theory with a determination of the model parameters. Finally, the results for $\langle S^2 \rangle$ are discussed in combination with those for $[\eta]$, giving attention to the Flory–Fox factor, Φ.

Experimental Section

Materials. The a-PS samples used in this work are mostly the same ones as used in the previous studies[1,2] on $\langle \Gamma^2 \rangle$ and $[\eta]$, i.e., the fractions separated from the standard samples supplied from Tosoh Co., Ltd., by preparative gel permeation chromatography (GPC) or fractional precipitation. They are sufficiently narrow in molecular weight distribution and have fixed stereochemical composition f_r independent of the molecular weight. The values of the weight-average molecular weight, M_w, obtained from light-scattering measurements are listed in Table I. The values of f_r determined by NMR, and the ratios of M_w to the number-average molecular weight, M_n, determined by GPC are given in the previous papers.[1,2] The latter were 1.02 for all of the additional samples F2, F4, and F10.

The solvent cyclohexane was purified by distillation after refluxing over sodium for about 6 h before each SAXS experiment. Test solutions were prepared gravimetrically and their polymer mass concentrations, c in g/cm^3, were calculated from their weight fractions with the solution density data obtained as described previously.[1,2]

Small-Angle X-ray Scattering. (i) Apparatus and Measurements. Our system for SAXS measurements is composed of X-ray tube (Phillips PW2253/11), Kratky U-slit camera (Anton Paar KA No. 1297), goniometer (Anton Paar ESW03 No. 6217) equipped with X-ray detector (scintillation counter probe), temperature control unit for a sample solution, water cycle system for cooling the X-ray tube, vacuum system, and

0024-9297/90/2223-0290$02.50/0 © 1990 American Chemical Society

Table I
Results of SAXS Measurements on Atactic Oligo- and Polystyrenes in Cyclohexane at 34.5 °C

			SAXS			
sample	M_w	x_w	$\langle S^2\rangle_s^{1/2}$, Å	$\langle S^2\rangle^{1/2}$, Å	φ_A', cm³/mol	M_w
OS5	578	5	4.7_5	3.3_9		588
OS6	680	5.98	5.1_4	3.9_2		629
OS8	904	8.13	5.8_9	4.8_7		888
A1000-b	1480	13.7	8.6_6	7.9_9	0.24_0	
A2500-a′	1780	16.6	9.9_9	9.4_2	0.26_4	
A2500-a	2270	21.3	$11._7$	$11._2$	0.26_2	
A2500-b	3480	32.9	$15._0$	$14._6$	0.28_1	
A5000-3	5380	51.2	$19._3$	$19._0$	0.25_9	
F1-2	10100	96.6	$27._5$	$27._3$	0.27_5	
F2	20500	197	$39._8$	$39._7$	0.27_3	
F4	40000	384	$56._7$	$56._6$	0.26_4	
F10	97300	935	$91._0$	$91._0$	0.28_1	

electric system (Rigaku Denki) for data acquisition and power supply to the X-ray tube. The camera and goniometer are mounted on an optical bench to allow for easy positioning and orienting of the incident X-ray beam. The optical bench and X-ray tube are tightly fixed on a heavy square plate made of iron, which is set on a rubber cushion to avoid vibrations. The whole system is installed in a temperature-controlled room (25 ± 1 °C) to keep the optical alignment in optimal setting so that the intensity of the X-ray beam impinged on the sample may not fluctuate. The temperature of cooling water supplied to the X-ray tube is also kept constant within ±0.5 °C for this purpose. It was confirmed that the temperature fluctuation in this range did not affect fluctuation in the intensity of the incident X-ray beam. The air in the path of the radiation is evacuated to prevent scattering from it.

The wavelength λ_0 of the X-ray from the source is mainly 1.54 Å (Cu Kα line) but slightly contaminated by Cu Kβ line and other weak radiation of different wavelengths. The pulse train due to the scattered X-ray at each scattering angle is thus registered in the counter and then printed out after passing through a pulse-height discriminator to eliminate the contamination, although the incident X-ray is monochromatized by the use of a Ni filter to eliminate the Cu Kβ line. The sample cell is a quartz capillary of inner diameter of 2.0 mm with a very thin wall (about 10 μm in thickness). Thus, test solutions have an optimum thickness for copper radiation, i.e., Cu Kα line. Collimation of the incident beam was carefully achieved to minimize the intensity of parasitic scattering and the tail of the transmitted X-ray. Preliminary measurements of scattering intensities from the solvent-filled and the empty cells showed that the intensities of these extra X-rays were negligibly small at angles beyond 5×10^{-3} rad and nullified down to about 1×10^{-3} rad by subtraction of the latter from the former. The lowest angle to which the cancellation was effected was dependent on the size of the entrance slit.

The intensity distributions $W_w(\theta_w)$ and $W_l(\theta_l)$ of the incident beam in two directions, i.e., the direction along the scattering angles (direction of the slit width) and the direction perpendicular to the scattering plane (direction of the slit length), respectively, were measured in the detector plane for later use in the desmearing of the experimental scattering function, $\tilde{I}(\tilde{\theta})$, or the correction for a finite size of the incident beam (slit width and length effect). Here, the angle $\tilde{\theta}$ is not the true scattering angle, θ, but the take-off angle through which the detector sees the sample. The zero take-off angle was defined as the peak position of the observed $W_w(\theta_w)$.

(ii) Data Acquisition and Analysis. Scattering intensities $\tilde{I}(\tilde{\theta})$ were measured at angles ranging from 1×10^{-3} rad up to the value at which the intensity became negligibly small. In most cases, the measurements were performed for five solutions of different concentrations and a solvent for each polymer sample. Corrections for stability of the X-ray source and the detector electronics were made by measuring the intensity scattered from Lupolene (a platelet of polyethylene) used as a working standard before and after each measurement for a given sample solution. The effect of absorption of X-ray by a given solution or solvent was also corrected by measuring the scattering intensity from Lupolene with inserting the solution or solvent in between the X-ray source and Lupolene. The obtained data were processed to desmear the observed (smeared) $\tilde{I}(\tilde{\theta})$ and then evaluate the molecular characteristics such as $\langle S^2\rangle_z$ and M_w. For this purpose, we introduce the reduced quantity $\tilde{I}_R(\tilde{\theta})$ defined by

$$\tilde{I}_R(\tilde{\theta}) = \tilde{I}(\tilde{\theta})/AI_0 \tag{1}$$

where A is the transmittance of a given sample and I_0 is the intensity of the incident beam monitored by the scattering intensity from Lupolene at 0.0103 rad. In practice, the excess reduced scattering intensity given by

$$\Delta\tilde{I}_R(\tilde{\theta}) = \tilde{I}_{R,soln}(\tilde{\theta}) - \tilde{I}_{R,solv}(\tilde{\theta}) \tag{2}$$

was subjected to the data processing. Here, the subscripts soln and solv denote the values of $\tilde{I}_R(\tilde{\theta})$ for a given solution and solvent, respectively.

An example of $\Delta\tilde{I}_R(\tilde{\theta})$ is displayed in Figure 1 for a cyclohexane solution of sample OS8 of $c = 0.1716$ g/cm³ at 34.5 °C as its inverse square root against $\tilde{k}^2$, where

$$\tilde{k} = (4\pi/\lambda_0)\sin(\tilde{\theta}/2) \tag{3}$$

The data points follow a curve slightly bent downward, approaching a straight line at small angles, although they scatter to some extent. We note that if the "observed" values (quasi data) $\Delta\tilde{I}_R$ are calculated (smeared) by the use of eq A2 in Appendix A with the functions $W_w(\theta_w)$ and $W_l(\theta_l)$ determined above and with the theoretical scattering functions $P(k) = \Delta I_R(\theta)$ for the Gaussian chain, rod, and sphere, which are given by[8]

$$P(k) = 2u^{-2}(e^{-u} - 1 + u) \quad \text{Gaussian chain} \tag{4}$$

$$P(k) = \frac{1}{(3u)^{1/2}}\mathrm{Si}[2(3u)^{1/2}] - \frac{1}{3u}\sin^2[(3u)^{1/2}] \quad \text{rod} \tag{5}$$

$$P(k) = \frac{243}{125u^3}\left[\sin\left(\frac{5u}{3}\right)^{1/2} - \left(\frac{5u}{3}\right)^{1/2}\cos\left(\frac{5u}{3}\right)^{1/2}\right]^2 \quad \text{sphere} \tag{6}$$

respectively, with $\mathrm{Si}(x)$ the sine integral and with

$$u = \langle S^2\rangle k^2 \tag{7}$$

$$k = (4\pi/\lambda_0)\sin(\theta/2) \tag{8}$$

then all of them also give straight lines at small angles in the (inverse) square-root plots, as seen from Figure 2. Thus we may expect that $[\Delta\tilde{I}_R(\tilde{\theta})]^{-1/2}$ follows a straight line at small angles irrespective of the form of the true (desmeared) $\Delta I_R(\theta)$. It then turns out that, in the desmearing of $\Delta\tilde{I}_R(\tilde{\theta})$, additional "data" points including the ordinate intercept may be obtained as those on the straight line fitted to the observed data points in order to make up for the lack of the observed values at very small angles.

The present desmearing procedure consists of expressing the true scattering function in terms of cubic B-spline functions, as described in Appendix A. Figure 3 shows errors in the scattering functions obtained by the desmearing of the "observed" data $\Delta\tilde{I}_R$ displayed in Figure 2. They are so small that this proce-

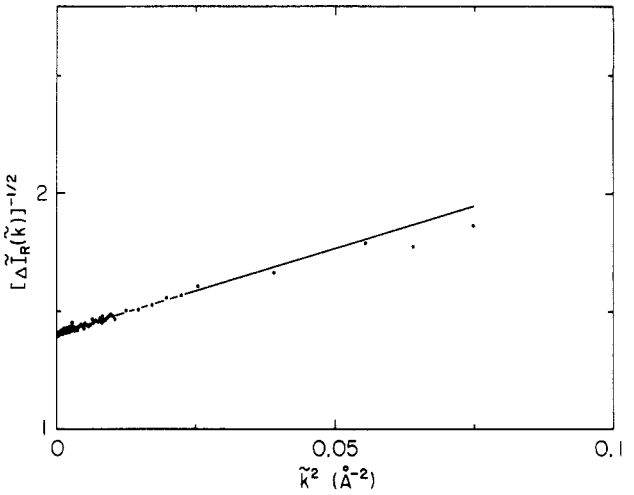

Figure 1. Inverse square-root plot of the excess reduced scattering intensity $\Delta\tilde{I}_R(\tilde{k})$ against $\tilde{k}^2$ for sample OS8 in cyclohexane (c = 0.1716 g/cm^3) at 34.5 °C. The straight line indicates the initial slope.

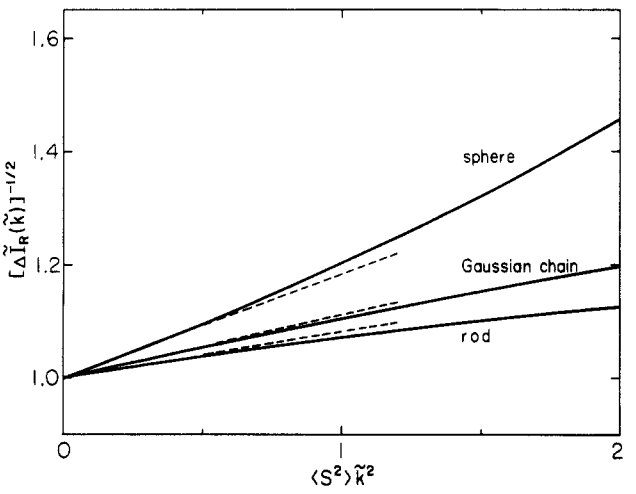

Figure 2. Inverse square-root plots of the "observed" values $\Delta\tilde{I}_R(\tilde{k})$ reduced by the respective ordinate intercepts against $\langle S^2\rangle\tilde{k}^2$ for the Gaussian chain, rod, and sphere. Solid curves, calculated from eq A2 with eq 4–6. Dashed straight lines, respective initial slopes.

dure may be applicable to various types of solute molecules. However, this requires some comments. For short chains, the effect of their finite thickness on the scattering intensity must be considered. The small oligomer molecules may then be approximated by the spheres. For our high molecular weight samples, on the other hand, the chains may be regarded as Gaussian with ignoring the thickness. Thus the above discussion is definitely valid for these two extremes, and this may be expected to be the case with their intermediates, for which the thickness cannot be ignored. All the data processing was done by the use of a FACOM M780 digital computer in this university.

The desmeared excess reduced intensities $\Delta I_R(\theta)$ were analyzed by the square-root plot[9] based on

$$\left[\frac{Kc}{\Delta I_R(\theta)}\right]^{1/2} = \left[\frac{1}{M_w P(k)}\right]^{1/2} + \mathcal{O}(c) \tag{9}$$

with

$$K = N_A I_e V \varphi_A \Delta z_e^2 \tag{10}$$

Here $P(k)$ is the scattering function given by

$$P(k) = 1 - (1/3)\langle S^2\rangle_s k^2 + \mathcal{O}(k^4) \tag{11}$$

This is rather the defining equation for $\langle S^2\rangle_s$. N_A is Avogadro's number, I_e is the Thomson factor (7.90 × 10^{-26} cm^2), V is the scattering volume, and φ_A is the apparatus constant dependent

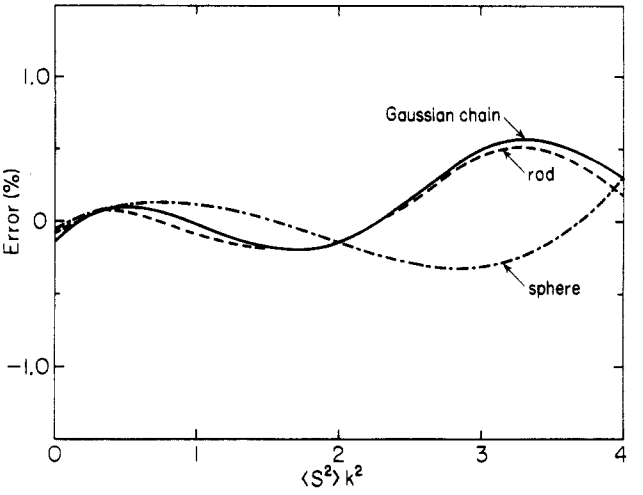

Figure 3. Differences (errors) between the original and desmeared scattering functions $P(k)$ as a function of $\langle S^2\rangle k^2$ for the Gaussian chain, rod, and sphere.

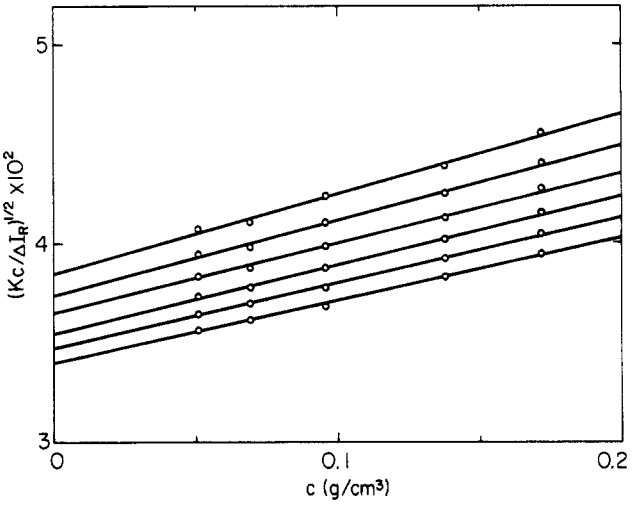

Figure 4. Plots of $(Kc/\Delta I_R)^{1/2}$ against c for sample OS8 in cyclohexane at 34.5 °C. The values of k^2 are 2.54, 1.97, 1.48, 1.01, 0.605, and 0.207 × 10^{-2} Å^{-2} from top to bottom.

on the sensitivity of the apparatus, the distance between the sample and detector, and so on. The mole number of effective electrons per gram of the sample solution Δz_e is defined by

$$\Delta z_e = (n_2/M_0 - \upsilon_2\rho_0 n_1/M_s) \tag{12}$$

where n_2 and M_0 are the number of electrons and the molecular weight per repeating unit of the polymer, respectively, υ_2 is the partial specific volume of the polymer, ρ_0 is the density of the solvent, and n_1 and M_s are the number of electrons and the molecular weight of the solvent molecule, respectively. The value 0.7653 g/cm^3 was used for ρ_0, and the value of υ_2 was determined for each sample from the density measurement for its cyclohexane solutions. All the measurements in this study were carried out at 34.5 °C, i.e., at the Θ temperature for a-PS in cyclohexane.

Viscometry. Intrinsic viscosities $[\eta]$ were determined for a-PS samples F2, F4, and F10 in cyclohexane at 34.5 °C following the procedure described previously.[2]

Results

Determination of $\langle S^2\rangle_s$. In Figures 4 and 5 are presented the data for the desmeared excess scattering intensity $\Delta I_R(\theta,c)$ on sample OS8 in cyclohexane at finite concentrations and angles in the form of the $(Kc/\Delta I_R)^{1/2}$ vs c and $(Kc/\Delta I_R)^{1/2}$ vs k^2 plots, respectively. Here the optical constant K was calculated from eq 10 with the apparatus constant φ_A' redefined by $\varphi_A' = N_A I_e V \varphi_A$. The value

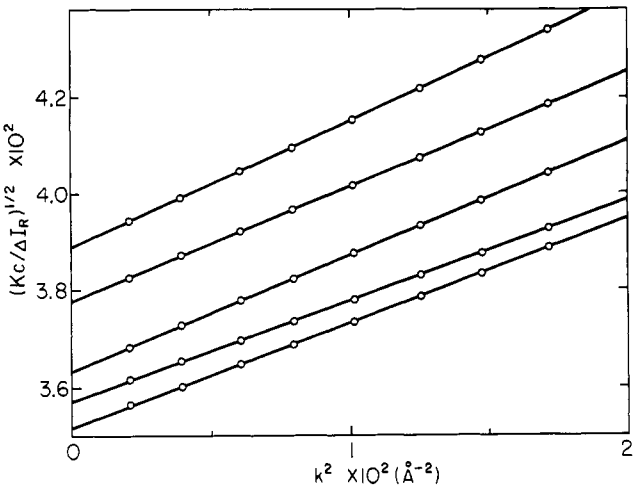

Figure 5. Plots of $(Kc/\Delta I_R)^{1/2}$ against k^2 for sample OS8 in cyclohexane at 34.5 °C. The polymer mass concentrations c are 0.1716, 0.1377, 0.0956, 0.0690, and 0.0508 g/cm³ from top to bottom.

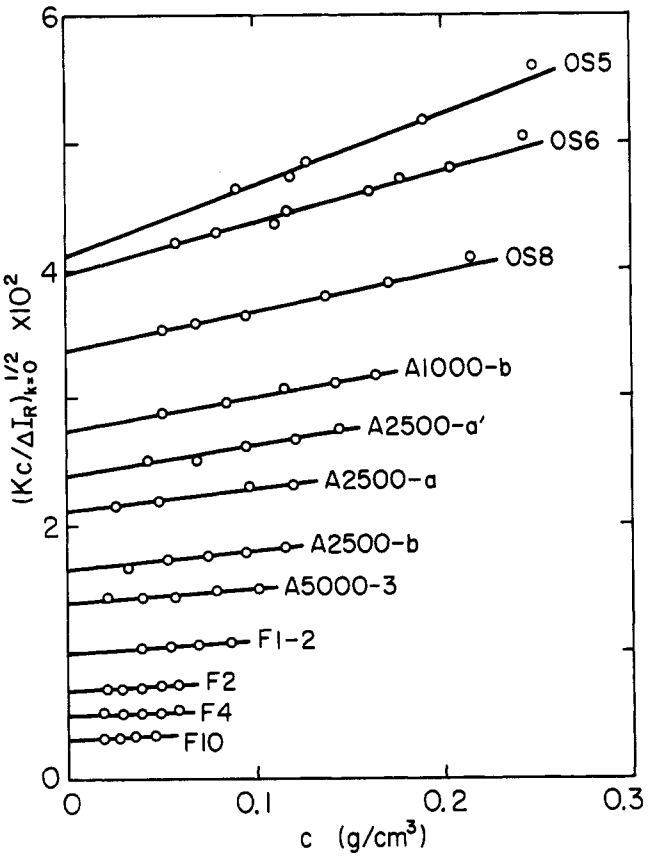

Figure 6. Plots of $(Kc/\Delta I_R)_{k=0}^{1/2}$ against c for the a-PS samples indicated in cyclohexane at 34.5 °C.

of φ_A' was determined so that the light-scattering values of M_w might be reproduced by the present analysis as described below. A set of data at fixed scattering angle k (Figure 4) and at fixed concentration c (Figure 5) are fitted by a straight line and can be easily extrapolated to zero concentration and zero scattering angle to evaluate $(Kc/\Delta I_R)_{c=0}^{1/2}$ and $(Kc/\Delta I_R)_{k=0}^{1/2}$, respectively. The values of $(Kc/\Delta I_R)_{k=0}^{1/2}$ and $(Kc/\Delta I_R)_{c=0}^{1/2}$ thus obtained are plotted against c and k^2 in Figures 6 and 7, respectively, for all the samples studied.

In Figure 6, the straight line fitted to the data points for each sample has a finite slope, indicating that the second virial coefficient, A_2, does not vanish for the a-

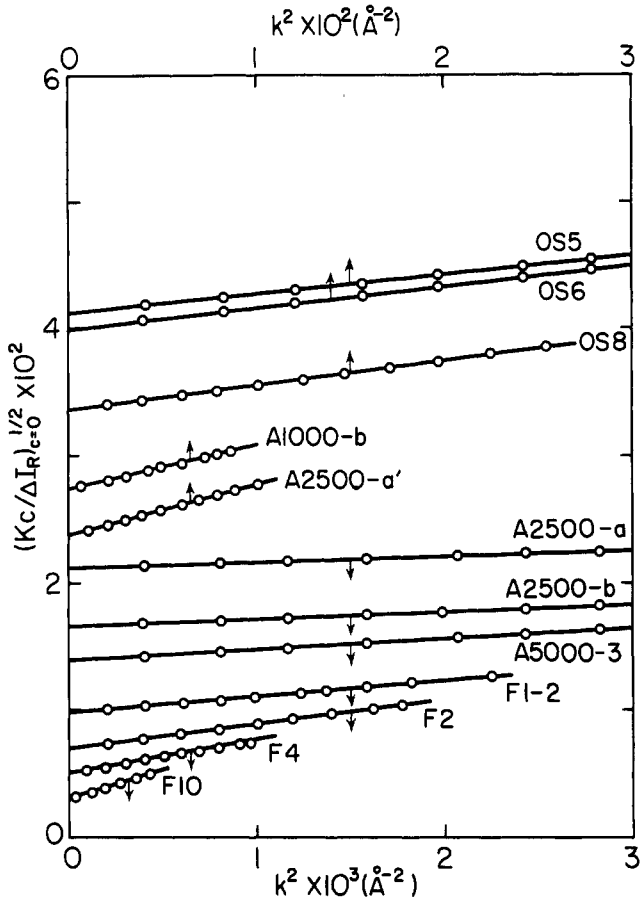

Figure 7. Plots of $(Kc/\Delta I_R)_{c=0}^{1/2}$ against k^2 for the a-PS samples indicated in cyclohexane at 34.5 °C.

PS oligomers even in the Θ state (cyclohexane at 34.5 °C). As seen from the figure, A_2 progressively decreases and tends to vanish with increasing molecular weight. This finding agrees qualitatively with that of Huber and Stockmayer.[10] However, we cannot argue the absolute values of A_2 themselves because of the large experimental uncertainty. (We will make an extensive study of A_2 in the future.) Nevertheless, we may at least say that the two-parameter theory of the excluded-volume effect seems to break down for $M_w \lesssim 10^5$, in which range the nonvanishing of A_2 is appreciable and $\langle S^2 \rangle$ deviates from the Gaussian behavior, as seen later. In Figure 7, the data points for each sample also follow the indicated straight line, and $\langle S^2 \rangle_s$ was evaluated from its slope. The straight line has an ordinate intercept coincident with that of the corresponding straight line drawn for the same sample in Figure 6. The apparatus constants φ_A' were determined from the intercepts of similar plots without φ_A' for the samples whose M_w had been obtained from light scattering, in advance of the plotting of Figures 6 and 7. For the oligomer samples OS5, OS6, and OS8, M_w's were determined from the respective common intercepts in Figures 6 and 7 with the use of the average value of φ_A' thus obtained.

The results from the present SAXS experiment are summarized in Table I. (For $\langle S^2 \rangle$, see the Discussion.) The values of $\langle S^2 \rangle_s^{1/2}$ range from 4.7_5 Å for the pentamer to $91._0$ Å for sample F10 of M_w = 97 300. The apparatus constants φ_A' determined for the samples other than the three oligomers are almost constant within the experimental error and have an average value of 0.26_6 cm³/mol. This indicates that our SAXS measurements are self-consistent. The SAXS values of M_w for the three oligomer samples OS5, OS6, and OS8 are in good agree-

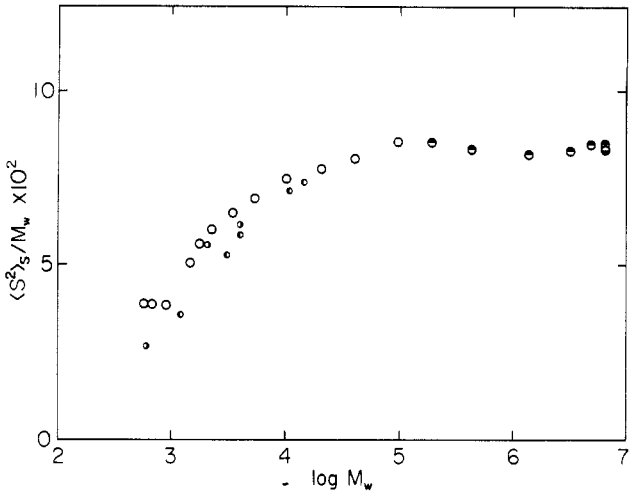

Figure 8. Molecular weight dependence of $\langle S^2\rangle_s/M_w$ for a-PS in cyclohexane at 34.5 °C ($\langle S^2\rangle_s$ in Å^2): ○, present data; ◑, SANS data by Ballard et al.;[13] ◐, SANS data by Huber et al.;[14,15] ◒, LS data by Miyaki;[12] ◒, LS data by Miyaki et al.[11]

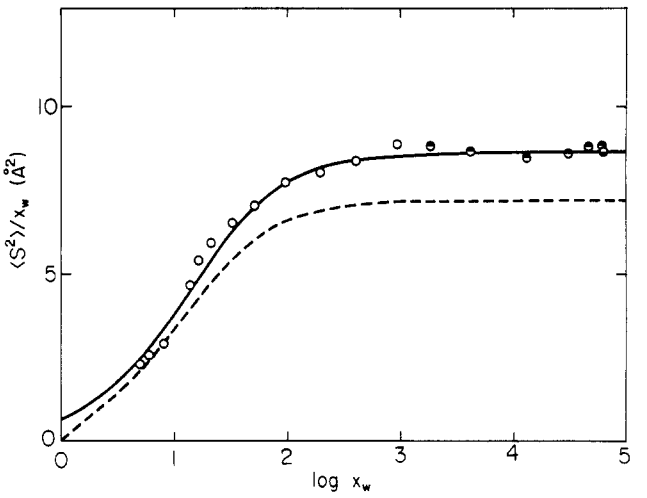

Figure 9. Ratio $\langle S^2\rangle/x_w$ as a function of the weight-average degree of polymerization, x_w, for a-PS with $f_r = 0.59$ in cyclohexane at 34.5 °C: ○, present data; ◒, LS data by Miyaki;[12] ◒, LS data by Miyaki et al.;[11] solid curve, best fit theoretical values calculated from eq 14; dashed curve, the RIS values.

ment with the calculated values (second column) obtained from the chemical structure and GPC analysis previously reported.[1,2]

Molecular Weight Dependence of $\langle S^2\rangle_s/M_w$. Figure 8 shows plots of the ratio $\langle S^2\rangle_s/M_w$ against the logarithm of M_w. It includes, for reference, the LS data by Miyaki et al.[11,12] for the a-PS samples of the same origin as ours in cyclohexane at 34.5 °C, and the SANS data for PS in cyclohexane-d_{12} at 38 °C by Ballard et al.[13] and at 35 °C by Huber et al.[14,15] The present data give a curve convex upward except for the two lowest molecular weight samples and are smoothly connected to the LS data, which are virtually constant, being independent of molecular weight. The values of $\langle S^2\rangle_s/M_w$ from SANS are however somewhat lower than ours when compared at fixed M_w. The origin of this discrepancy is not clear at present. The results from the present SAXS measurements combined with the LS data by Miyaki et al. lead to the conclusion that the ratio $\langle S^2\rangle_s/M_w$ increases with increasing M_w for $M_w \lesssim 10^5$ and then levels off to yield a constant value of 8.3×10^{-18} cm^2·mol/g.[11]

Discussion

Determination of $\langle S^2\rangle$. The values of $\langle S^2\rangle_s$ determined above contain contributions from the finite cross section of the polymer chain. The effect must be taken into account when the molecular weight dependence of the mean-square radius of gyration, $\langle S^2\rangle$, is discussed, since the theoretical evaluation of the latter has been carried out for the chain contour. As shown in Appendix B, $\langle S^2\rangle_s$ determined directly by scattering methods with eq 11 may be expressed as

$$\langle S^2\rangle_s = \langle S^2\rangle + S_c^2 \tag{13}$$

for a discrete model chain composed of subbodies with finite volumes or a continuous chain with a finite cross section with S_c the radius of gyration for the subbody or cross section.

According to our previous study[2] on a-PS by viscometry, the a-PS chain may be represented by either of the two models, i.e., the HW touched-bead model with bead diameter, d_b, of 10.1 Å or the HW cylinder model with diameter, d, of 7.5 Å. For the cylinder model, d may also be calculated to be 9.2 Å from $d = 2(v_2 M_L/\pi N_A)^{1/2}$ with $v_2 = 0.934$ cm^3/g at sufficiently large M_w and with $M_L = 42.6$ Å^{-1} obtained previously. From these values, S_c^2 are calculated from eq B6 or B8 to be 15.3, 7.0, and 10.5 Å^2, respectively. We adopted 11 Å^2 as their average for S_c^2 in this work. The contribution of S_c^2 to $\langle S^2\rangle_s$ amounts to about 50% for the pentamer but progressively diminishes with increasing molecular weight and becomes negligible at M_w larger than 2×10^4.

The results of $\langle S^2\rangle$ thus calculated from eq 13 are given in Table I and shown in Figure 9 in the form of the $\langle S^2\rangle/x_w$ vs log x_w plot (with x_w the weight-average degree of polymerization). In this figure, the values from the LS experiments by Miyaki et al.[11,12] are again included to supplement the data at x_w larger than the range accessible by SAXS. The dashed curve represents the theoretical values of $\langle S^2\rangle$ for the x α-carbon atoms calculated on the basis of the rotational isomeric state (RIS) model. The RIS calculations were made by the Monte Carlo method established by Flory[16,17] with the generator matrix given in Appendix C and use was made of the statistical weight matrices and the molecular parameters given in the previous paper.[1] The calculated values may well explain the observed behavior of $\langle S^2\rangle/x_w$ at x_w smaller than 10. This also implies that the present correction for the finite cross section is rather reasonable, since the RIS value for $x = 2$ is exactly correct. However, the RIS values deviate appreciably downward from the experimental values at larger x_w and approach an asymptotic value lower than the observed result by about 17%. A similar result was also found for $\langle \Gamma^2\rangle$ in our previous study.[1] The discrepancy suggests that the rotational isomeric states and/or the energy parameters in the statistical weight matrices adopted by Yoon et al.[18] should be reconsidered.

Values of the HW Model Parameters. For the HW chain of contour length L (with vanishing Poisson's ratio, σ), $\langle S^2\rangle$ is given by[6,19]

$$\langle S^2\rangle = \frac{\tau_0^2}{\nu^2}\langle S^2\rangle_{KP} + \frac{\kappa_0^2}{\nu^2}\left[\frac{L}{3r}\cos\varphi - \frac{1}{r^2}\cos(2\varphi) + \frac{2}{r^3 L}\cos(3\varphi) - \frac{2}{r^4 L^2}\cos(4\varphi) + \frac{2}{r^4 L^2}e^{-2L}\cos(\nu L + 4\varphi)\right] \tag{14}$$

with

$$\nu = (\kappa_0^2 + \tau_0^2)^{1/2} \quad (15)$$

$$r = (4 + \nu^2)^{1/2} \quad (16)$$

$$\varphi = \cos^{-1}(2/r) \quad (17)$$

and

$$\langle S^2\rangle_{KP} = L/6 - 1/4 + 1/4L - (1/8L^2)(1 - e^{-2L}) \quad (18)$$

where all lengths have been reduced by λ^{-1} and $\langle S^2\rangle_{KP}$ is the mean-square radius of gyration for the Kratky–Porod (KP) wormlike chain having the same L as the HW chain. The basic HW model parameters necessary to represent the unreduced (or experimental) $\langle S^2\rangle$ are then κ_0, τ_0, λ^{-1}, and M_L. These parameters can be determined from a comparison of the theoretical values of $\langle S^2\rangle$ as a function of chain length, L, with the observed values of $\langle S^2\rangle$ as a function of M_w. The solid curve in Figure 9 represents the theoretical values best fit to the experimental data. It is seen that the curve describes quantitatively the behavior of $\langle S^2\rangle/x_w$ as a function of x_w over the whole range of molecular weight examined. We have not made an analysis of the data on the basis of the KP model, since it fails to give a consistent explanation of $\langle S^2\rangle$, $\langle \Gamma^2\rangle$, and $[\eta]$, as discussed previously.[2]

The values of the model parameters thus determined are summarized in Table II together with those obtained from $\langle \Gamma^2\rangle$ and $[\eta]$ in the same solvent condition, for comparison. It is to be noted that κ_0 and τ_0 in the table are reduced by λ^{-1}. The present values of λ^{-1} and M_L are very close to those from $\langle \Gamma^2\rangle$ but somewhat smaller than those from $[\eta]$. In this connection, it is pertinent here to make some comments on the analysis of the $[\eta]$ data by the viscosity theory[4,5] for the HW model. The theory gives 2.87×10^{23} mol^{-1} for the Flory–Fox factor, Φ_∞, at infinite chain length (see below), while its best experimental value determined so far[11] for a-PS in cyclohexane at Θ is $2.5_5 \times 10^{23}$ mol^{-1}. The differences between the values of λ^{-1} and M_L obtained from $\langle S^2\rangle$ and $[\eta]$ may be regarded as mainly arising from this difference in Φ_∞.

The radius, ρ, and pitch, h, of the characteristic regular helix of the HW chain are related to the (unreduced) κ_0 and τ_0 by $\rho = \kappa_0/(\kappa_0^2 + \tau_0^2)$ and $h = 2\pi\tau_0/(\kappa_0^2 + \tau_0^2)$, respectively. The values of ρ and h for the a-PS chain were calculated to be 1.50 and 18.8 Å, respectively, from the values of κ_0, τ_0, and λ^{-1} given in Table II. It is interesting to give some preliminary discussion of the results in comparison with those for atactic poly(methyl methacrylate) (a-PMMA) obtained from $\langle S^2\rangle$ in acetonitrile.[20] The results indicate that the characteristic helix of a-PS is more highly extended along the helix axis, having smaller ρ and larger h, than that of a-PMMA. The extent to which the helical form is preserved in solution is lower in the a-PS chain than in the a-PMMA chain, considering from their values of λ^{-1}. The results for a-PMMA will soon be published.[20]

Flory–Fox Factor Φ. In order to discuss the present results for $\langle S^2\rangle$ in connection with those for $[\eta]$ reported previously, we calculated the Flory–Fox factor, Φ, from the relation

$$[\eta] = 6^{3/2}\Phi\langle S^2\rangle^{3/2}/M_w \quad (19)$$

The results are given in Table III, and the ratios of Φ to Φ_∞ are double-logarithmically plotted against M_w in Figure 10, where the values calculated from Miyaki et al.'s data[11,12] are again included. The value 2.55×10^{23} mol^{-1} was used here for Φ_∞. The ratio Φ/Φ_∞ is substantially constant at M_w higher than 10^5 but steeply increases as M_w decreases from 10^5, in contrast to the widely accepted notion that Φ should decrease with decreasing chain length because of the draining effect, i.e., the decrease in the hydrodynamic interaction in a polymer chain. The rise of Φ/Φ_∞ at small M_w is due to two factors: One is the decrease in the ratio $\langle S^2\rangle/M_w$ and the other is the increase in $[\eta]$ deviating from the relation $[\eta] \propto M_w^{1/2}$. For a-PS in cyclohexane at Θ, $\langle S^2\rangle/M_w$ decreases with decreasing M_w at M_w lower than 10^5 as seen from Figure 9, and $[\eta]$ follows the relation $[\eta] \propto M_w^{1/2}$ over a wide range of M_w above 4000 and deviates upward from this relation at lower M_w as reported previously.[2] Thus, the increase in Φ/Φ_∞ in the range of M_w from 10^5 to 4000 results solely from the first factor and the further increase at lower M_w from both of them. In general, it is anticipated that the ratio Φ/Φ_∞ depends on molecular weight in a subtle way depending on competitive overlapping of the two factors.

Table II
Values of the HW Model Parameters for Atactic Polystyrene with $f_r = 0.59$ in Cyclohexane at 34.5 °C

κ_0	τ_0	λ^{-1}, Å	M_L, Å^{-1}	obs
(3.0)	(6.0)	22.5	36.7	$\langle S^2\rangle$
3.0	6.0	22.7	37.1	$\langle \Gamma^2\rangle$
(3.0)	(6.0)	23.5	42.6	$[\eta]$

Table III
Values of the Flory–Fox Factor, Φ

sample	$[\eta]$, dL/g	$\Phi \times 10^{-23}$, mol^{-1}
OS5	0.0274[a]	27.6
OS6	0.0293[a]	22.4
OS8	0.0326[a]	17.4
A1000-b	0.0370[a]	7.29
A2500-a′	0.0408[a]	5.91
A2500-a	0.0450[a]	4.97
A2500-b	0.0543[a]	4.10
A5000-3	0.0659[a]	3.53
F1-2	0.0900[a]	3.06
F2	0.123	2.73
F4	0.172	2.57
F10	0.273	2.40

[a] Previously reported.[2]

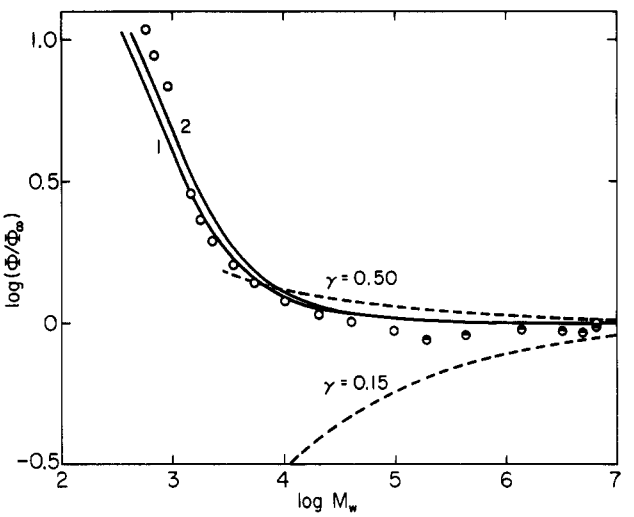

Figure 10. Molecular weight dependence of the Flory–Fox factor, Φ, reduced with Φ_∞ for a-PS with $f_r = 0.59$ in cyclohexane at 34.5 °C: ○, present data; ◓, Miyaki's data;[12] ◒, Miyaki et al.'s data;[11] solid curves, the HW values calculated with $\kappa_0 = 3.0$, $\tau_0 = 6.0$, $\lambda^{-1} = 22.5$ Å, and $M_L = 36.7$ Å^{-1} (1) and $\kappa_0 = 3.0$, $\tau_0 = 6.0$, $\lambda^{-1} = 23.5$ Å, and $M_L = 42.6$ Å^{-1} (2); dashed curves, the Gaussian theory[21] values calculated with the indicated γ.

The solid curves 1 and 2 in Figure 10 represent the values of Φ/Φ_∞ calculated for the HW chain with the two sets of the model parameters: $\kappa_0 = 3.0$, $\tau_0 = 6.0$, $\lambda^{-1} = 22.5$ Å, and $M_L = 36.7$ Å^{-1} from $\langle S^2\rangle$ and $\kappa_0 = 3.0$, $\tau_0 = 6.0$, $\lambda^{-1} = 23.5$ Å, and $M_L = 42.6$ Å^{-1} from $[\eta]$, respectively. The agreement between the calculated and observed Φ/Φ_∞ is almost quantitative. The dashed curves are the Yamakawa theory predictions[21] for Gaussian chains with the indicated values of γ, where γ is the ratio of the bead diameter to the effective bond length. We assigned the effective bond length a value 18.4 Å calculated as the Kuhn statistical segment length A_K from the HW model parameters determined in this work and converted the number of beads in the Gaussian chain model to the molecular weight so that the experimental value of $\langle S^2\rangle/M_w$ in the limit of large M_w might be reproduced. It is seen that these theoretical values of Φ/Φ_∞ deviate upward or downward from unity, depending on the value of γ, already at very large M_w far above 10^7, in contrast to the observed behavior. We note that the curve with $\gamma = 0.5$ indicates nearly the upper bound on Φ/Φ_∞ (at each M_w). The ratio increases gradually with decreasing molecular weight but does not exhibit any trend of a sharp increase in it found experimentally. In this theory, the increase in Φ/Φ_∞ is due only to the upward deviation of $[\eta]$ from the relation $[\eta] \propto M_w^{1/2}$, since $\langle S^2\rangle/M$ is independent of M for the Gaussian chain. (This deviation of $[\eta]$ arises from the consideration of the finiteness of the number of effective bonds in the Gaussian chain.[21]) The breakdown of the Gaussian theory in this region is then rather natural, since it fails to describe the conformational behavior of the real chain of any length, as is clearly seen from Figure 9. In the present case, it is important to recall that the Gaussian behavior breaks down for $\langle S^2\rangle$ for $M_w \lesssim 10^5$, while it *apparently* persists for $[\eta]$ down to $M_w = 4000$.

In conclusion, the present consistent explanation of $\langle S^2\rangle$ and $[\eta]$ of a-PS adds further support to the adequacy of the adaptation of the HW chain model to it over a wide range of molecular weight. The forthcoming analysis of the data for a-PMMA[20] will provide our more profound understanding of the conformational behavior of the real chain on the basis of the HW model.

Appendix A. Desmearing of the Experimental Scattering Function

Although the desmearing procedure we used is essentially the same as that developed by Glatter,[7] we give its short sketch, for convenience. The observed excess reduced scattering intensity, $\Delta\tilde{I}_R(\tilde{\theta})$, at a take-off angle $\tilde{\theta}$ may be related to the true excess reduced scattering intensity, $\Delta I_R(\theta)$, at a scattering angle θ as

$$\Delta\tilde{I}_R(\tilde{\theta}) = \int_{-\infty}^{\infty} d\theta_w \int_{-\infty}^{\infty} d\theta_l\, W_w(\theta_w)\, W_l(\theta_l)\, \Delta I_R([(\tilde{\theta} - \theta_w)^2 + \theta_l^2]^{1/2}) \quad \text{(A1)}$$

where $W_w(\theta_w)$ and $W_l(\theta_l)$ are the normalized slit-width and slit-length weighting functions, respectively, which can be determined experimentally. It is convenient to rewrite eq A1 in the form

$$\Delta\tilde{I}_R(\tilde{\theta}) = \int_0^{\infty} K(\tilde{\theta}, \theta)\, \Delta I_R(\theta)\, \theta\, d\theta \quad \text{(A2)}$$

with $K(\tilde{\theta}, \theta)$ the kernel defined by

$$K(\tilde{\theta}, \theta) = 2\int_0^{\pi} W_w(\tilde{\theta} - \theta\cos\varphi) W_l(\theta\sin\varphi)\, d\varphi \quad \text{(A3)}$$

Mathematically, the integral eq A2 for ΔI_R cannot be solved rigorously with experimental data for $\Delta\tilde{I}_R$ obtained in a finite range of $\tilde{\theta}$. However, its sufficiently accurate solution may be obtained at small θ in the following way, since $\Delta I_R(\theta)$ with small $|\tilde{\theta} - \theta|$ makes its main contribution to $\Delta\tilde{I}_R(\tilde{\theta})$ at a given $\tilde{\theta}$.

We expand $\Delta I_R(\theta)$ in terms of a set of cubic B-spline functions $M_i(x; \xi_i, \xi_{i+1}, ..., \xi_{i+4})$ $(i = 1\text{–}n)$ by Schoenberg's definition[22] with a set of knots $(\xi_1, \xi_2, ..., \xi_{n+4})$ as

$$\Delta I_R(\theta) = \sum_{i=1}^{n} a_i M_i(\theta^2; \xi_i, \xi_{i+1}, ..., \xi_{i+4}) \quad \text{(A4)}$$

Note that we have chosen θ^2 instead of θ itself as the argument of M, since ΔI_R is an even function of θ. Further, we note that the first four knots, ξ_1, ξ_2, ξ_3, and ξ_4, are set equal to zero. The expansion coefficients a_i $(i = 1\text{–}n)$ and the knots ξ_i $(i = 5, ..., n + 4)$ are determined by the method of least squares for $\Delta\tilde{I}_R$. The residual sum of the squares is a nonlinear function of the knots, and this nonlinear problem is solved by the quasi-Newton method. The integrations appearing on the right-hand sides of eq A2 and A3 are carried out numerically by the use of the trapezoidal rule formula. The optimal number n of the B-spline functions are determined by the use of Akaike's information criterion,[23] as done by Hiragi et al.[24]

Appendix B. Correction for $\langle S^2\rangle_s$ for an Assembly of Scatterers with Finite Volumes

The scattering function $P(\mathbf{k})$ with $\mathbf{k}$ the scattering vector may be written in the form

$$P(\mathbf{k}) = \langle |\int \rho(\mathbf{r}) e^{i\mathbf{k}\cdot\mathbf{r}}\, d\mathbf{r}|^2\rangle \quad \text{(B1)}$$

where i is the imaginary unit and $\rho(\mathbf{r})$ is the excess electron density at vector position $\mathbf{r}$ normalized as

$$\int \rho(\mathbf{r})\, d\mathbf{r} = 1 \quad \text{(B2)}$$

We consider two types of the electron distribution. One is an assembly of N identical subbodies of volume v_s in which the electrons distribute uniformly, and the other is a uniform distribution within a flexible cylinder of contour length L having a uniform normal cross section of area a_c whose center of mass is on the contour.

For the former, ρ may be expressed as

$$\rho(\mathbf{r}) = (Nv_s)^{-1} \sum_{p=1}^{N} \int_{V_p} \delta(\mathbf{r} - \mathbf{R}_p - \mathbf{r}_p)\, d\mathbf{r}_p \quad \text{(B3)}$$

where $\mathbf{R}_p$ is the vector position of the center of mass of the pth subbody, $\mathbf{r}_p$ is the vector distance from $\mathbf{R}_p$ to an arbitrary point within the pth subbody, $\delta(\mathbf{r})$ is the three-dimensional Dirac δ function, and $\int_{V_p} d\mathbf{r}_p$ indicates the integration within the pth subbody. For the latter, ρ may be expressed as

$$\rho(\mathbf{r}) = (La_c)^{-1} \int_0^L dt \int_{c_t} \delta[\mathbf{r} - \mathbf{R}(t) - \mathbf{r}_t]\, d\mathbf{r}_t \quad \text{(B4)}$$

where $\mathbf{R}(t)$ is the vector position of the contour point t, $\mathbf{r}_t$ is the vector distance from $\mathbf{R}(t)$ to an arbitrary point in the normal cross section at the contour point t, and $\int_{c_t} d\mathbf{r}_t$ indicates the integration over the cross section.

Substituting eq B3 into eq B1, expanding eq B1 in powers of $\mathbf{k}$, and taking the average over the entire orientation, we obtain eq 11 with eq 13 for the former case. In eq 13, $\langle S^2\rangle$ is the mean-square radius of gyration for the centers of masses of the N subbodies (on the chain contour) and is given by

$$\langle S^2\rangle = (2N^2)^{-1} \sum_{p,q=1}^{N} \langle R_{pq}^2\rangle \quad \text{(B5)}$$

where R_{pq} is the distance between the centers of masses of the pth and qth subbodies, and S_c in eq 13 is the radius of gyration of the subbody. For example, if it is the spherical bead of diameter d_b, S_c is given by

$$S_c = (15)^{1/2} d_b/10 \tag{B6}$$

For the latter case, we obtain the same expression as eq 11 with eq 13 by the use of eq B4 in place of eq B3. In this case, $\langle S^2 \rangle$ in eq 13 is the mean-square radius of gyration for the contour and is given by

$$\langle S^2 \rangle = (2L^2)^{-1} \int_0^L \int_0^L \langle R_{st}^2 \rangle \, ds \, dt \tag{B7}$$

where R_{st} is the distance between the contour points s and t, and S_c in eq 13 is the radius of gyration of the normal cross section and is given by

$$S_c = (2)^{1/2} d/4 \tag{B8}$$

with d the cylinder diameter.

Appendix C. $\langle S^2 \rangle$ of the RIS Model Chain

We consider the mean-square radius of gyration $\langle S^2 \rangle$ for a subset consisting of properly chosen main-chain carbon atoms (with equal mass) on the basis of the RIS model. Let ϵ_i (i = 0–n) be the parameter such that $\epsilon_i = 1$ if the ith carbon atom belongs to the subset and $\epsilon_i = 0$ otherwise. $\langle S^2 \rangle$ for the subset may then be written in the form

$$\langle S^2 \rangle = \left(\sum_{i=0}^{n} \epsilon_i\right)^{-2} \sum_{i=0}^{n-1} \sum_{j=i+1}^{n} \epsilon_i \epsilon_j \langle R_{ij}^2 \rangle \tag{C1}$$

with R_{ij} the distance between the ith and jth carbon atoms. The mean-square radius of gyration $\langle S^2 \rangle$ thus defined may easily be calculated following the matrix algebra developed by Flory[16,17] for the RIS moments only by replacing the generator matrix $\mathbf{S}_i$ (i = 1–n) defined by eq 27 of ref 17 by

$$\mathbf{S}_i = \begin{pmatrix} 1 & \delta_{i1}(\epsilon_0 - 1) + \epsilon_i & 2c_i \mathbf{l}_i^{\mathrm{T}} \cdot \mathbf{T}_i & c_i l_i^2 & c_i \epsilon_i l_i^2 \\ 0 & 1 & 2\mathbf{l}_i^{\mathrm{T}} \cdot \mathbf{T}_i & l_i^2 & \epsilon_i l_i^2 \\ \mathbf{0} & \mathbf{0} & \mathbf{T}_i & \mathbf{l}_i & \epsilon_i \mathbf{l}_i \\ 0 & 0 & \mathbf{0} & 1 & \epsilon_i \\ 0 & 0 & \mathbf{0} & 0 & 1 \end{pmatrix} \tag{C2}$$

Here, δ_{ij} is the Kronecker δ, c_i is given by

$$c_i = 1 - \delta_{i1} + \delta_{i1}\epsilon_0 \tag{C3}$$

$\mathbf{T}_i$ is the transformation matrix from the (i + 1)th localized coordinate system affixed to the (i + 1)th skeletal bond to the ith one, $\mathbf{l}_i$ is the ith bond vector expressed in the ith coordinate system, $l_i = |\mathbf{l}_i|$, and the superscript T indicates the transpose. Note that $\mathbf{S}_i$ given by eq C2 becomes identical with that defined in ref 17 if all ϵ_i are set equal to unity.

For the calculation of $\langle S^2 \rangle$ for the set of α-carbon atoms, in which we are interested, we may choose $\epsilon_i = 1$ if the ith skeletal carbon is the α-carbon and $\epsilon_i = 0$ otherwise.

References and Notes

(1) Konishi, T.; Yoshizaki, T.; Shimada, J.; Yamakawa, H. *Macromolecules* **1989**, *22*, 1921.
(2) Einaga, Y.; Koyama, H.; Konishi, T.; Yamakawa, H. *Macromolecules* **1989**, *22*, 3419.
(3) Yamakawa, H.; Fujii, M.; Shimada, J. *J. Chem. Phys.* **1979**, *71*, 1611.
(4) Yamakawa, H.; Yoshizaki, T. *Macromolecules* **1980**, *13*, 633.
(5) Yoshizaki, T.; Nitta, I.; Yamakawa, H. *Macromolecules* **1988**, *21*, 165.
(6) Yamakawa, H. In *Molecular Conformation and Dynamics of Macromolecules in Condensed Systems*; Nagasawa, M., Ed., Elsevier: Amsterdam, The Netherlands, 1988; p 21.
(7) Glatter, O.; Kratky, O. *Small Angle X-ray Scattering*; Academic Press: New York, 1982.
(8) Yamakawa, H. *Modern Theory of Polymer Solutions*; Harper & Row: New York, 1971.
(9) Berry, G. C. *J. Chem. Phys.* **1966**, *44*, 4550.
(10) Huber, K.; Stockmayer, W. H. *Macromolecules* **1987**, *20*, 1400.
(11) Miyaki, Y.; Einaga, Y.; Fujita, H.; Fukuda, M. *Macromolecules* **1980**, *13*, 588.
(12) Miyaki, Y. Ph.D. Thesis, Osaka University, 1981.
(13) Ballard, D. G. H.; Rayner, M. G.; Shelten, J. *Polymer* **1976**, *17*, 349.
(14) Huber, K.; Bantle, S.; Lutz, P.; Burchard, W. *Macromolecules* **1985**, *18*, 1461.
(15) Huber, K.; Burchard, W.; Bantle, S. *Polymer* **1987**, *28*, 863.
(16) Flory, P. J. *Statistical Mechanics of Chain Molecules*; Interscience: New York, 1969.
(17) Flory, P. J. *Macromolecules* **1974**, *7*, 381.
(18) Yoon, D. Y.; Sundararajan, P. R.; Flory, P. J. *Macromolecules* **1975**, *8*, 776.
(19) Yamakawa, H.; Fujii, M. *J. Chem. Phys.* **1976**, *64*, 5222.
(20) Tamai, Y.; Konishi, T.; Einaga, Y.; Fujii, M.; Yamakawa, H., to be published in *Macromolecules*.
(21) Yamakawa, H. *J. Chem. Phys.* **1970**, *53*, 436.
(22) Greville, T. N. E. In *Theory and Applications of Spline Functions*; Greville, T. N. E., Ed.; Academic Press: New York, 1969; p 1.
(23) Akaike, H. *IEEE Trans. Autom. Control* **1974**, *AC-19*, 716.
(24) Hiragi, Y.; Urakawa, H.; Tanabe, K. *J. Appl. Phys.* **1985**, *58*, 5.